Table IV. Theoretical values calculated for the diffusion-controlled reaction are also shown in the parentheses. In the case of $\Delta G^{\ddagger}$, the experimental results are in good agreement with the theoretical values. As for $\Delta H^{\ddagger}$ and $\Delta S^{\ddagger}$, however, the experimental values are larger than the theoretical values. The $\Delta H^{\ddagger}$ value is larger because there is a rate-determining factor that needs a large activation energy in the association reaction. Dehydration of latex particles in the association process as suggested by previous authors[17-19] and conformational changes of charged side chains on the latex surface are possible reasons for the larger experimental values of $\Delta H^{\ddagger}$ and $\Delta S^{\ddagger}$.

(17) Johnston, G. A.; Lecchini, A. M. A.; Smith, E. G.; Clifford, J.; Pethica, B. A. *Discuss. Faraday Soc.* **1966**, *42*, 120.
(18) Lichtenbelt, J. W. T.; Ras, H. J. M. C.; Wieserma, P. H. *J. Colloid Interface Sci.* **1974**, *46*, 522.
(19) Lichtenbelt, J. W. T.; Pathmamanoharan, C.; Wieserma, P. H. *J. Colloid Interface Sci.* **1974**, *49*, 281.

Excimer Laser Photolysis of V(CO)₆: Time-Resolved Infrared Studies of Gas-Phase V(CO)ₓ (x = 5-2)[†]

Y. Ishikawa,[‡] P. A. Hackett, and D. M. Rayner*

Contribution from the Laser Chemistry Group, Division of Chemistry, National Research Council, Ottawa, Ontario K1A 0R6, Canada. Received March 10, 1987

Abstract: The photolysis of gas-phase vanadium hexacarbonyl, $V(CO)_6$, has been studied at excimer laser wavelengths (351, 308, 248, and 193 nm) by observing the coordinatively unsaturated transient products, $V(CO)_x$ ($x = 5-3$ and possibly 2), via time-resolved infrared kinetic absorption spectroscopy. The dependence of the initial fragment distribution on photolysis wavelength is consistent with the model of sequential CO elimination established by similar studies on $Fe(CO)_5$, $Cr(CO)_6$, and $Co(CO)_3NO$. The high reactivity of unsaturated metal carbonyl species with saturated carbonyls to form binuclear complexes is again observed, with rate constants for the reaction of $V(CO)_3$ and $V(CO)_4$ with $V(CO)_6$ found to be of the order 3×10^{-10} cm³ molecule⁻¹ s⁻¹. Infrared assignments for $V(CO)_x$ are supported by kinetic measurements in the presence of added CO. Rate constants for the reaction of CO with $V(CO)_3$, $V(CO)_4$, and $V(CO)_5$ are found as $(0.4 \pm 0.1) \times 10^{-10}$, $(0.5 \pm 0.1) \times 10^{-10}$, and $(0.5 \pm 0.1) \times 10^{-10}$ cm³ molecule⁻¹ s⁻¹, respectively, leading to the expectation that ground-state $V(CO)_{3-5}$ share the doublet character of $V(CO)_6$. The infrared assignments are in disagreement with infrared absorption and some ESR studies of $V(CO)_x$ fragments in low-temperature matrices.

The general chemistry of coordinatively unsaturated transition-metal carbonyl species is of major interest due to the demonstrated role of individual species as active catalytic agents.[1-7] Vanadium is one of the limited list of transition metals whose unsaturated binary carbonyls have been reported to have been isolated in low-temperature rare-gas matrices and studied by both infrared absorption and ESR. $V(CO)_5$ was first reported to have been observed by infrared absorption consistent with a D_{3h} geometry following the in situ matrix photolysis of $V(CO)_6$.[8] Ozin and co-workers observed infrared absorptions attributed to $V(CO)_{1-6}$ following vanadium atom/CO co-condensation experiments.[9] Their results are in disagreement with later ESR studies of Morton and Preston on the matrix-isolated species formed following the in situ γ-radiolysis of $V(CO)_6$.[10] These species were assigned as $V(CO)_5$ and $V(CO)_4$, but their reported geometries are at odds with Ozin and co-workers' infrared assignments. Recent ESR measurements by Weltner and co-workers on the lower members of the series, $V(CO)_{1-3}$, formed by co-condensation at 4 K, are also in disagreement with the early matrix infrared absorption work.[11]

Time-resolved infrared absorption techniques have recently been developed which now allow the study of coordinatively unsaturated transient species formed following the ultraviolet photolysis of metal carbonyls in both gas[12-16] and solution phases.[17-20] Weitz and co-workers have reported comprehensive studies, including photolysis wavelength dependence, on the photolysis of $Fe(CO)_5$,[12] $Cr(CO)_6$,[13] and $Mn_2(CO)_{10}$.[14] Fletcher and Rosenfeld have in-

(1) Geoffroy, G. L.; Wrighton, M. S. *Organometallic Photochemistry*; Acaedemic: New York, 1979.
(2) Wrighton, M. S.; Ginley, D. S.; Schroeder, M. A.; Morse, D. L. *Pure Appl. Chem.* **1975**, *41*, 671.
(3) Wrighton, M. S.; Graff, J. L.; Kazlansleas, R. J.; Mitchener, J. C.; Reichel, C. L. *Pure Appl. Chem.* **1982**, *54*, 161.
(4) Whetten, R. L.; Grant, E. R. *J. Am. Chem. Soc.* **1982**, *104*, 4270.
(5) Tumas, W.; Gitlin, B.; Rosan, A. M.; Yardley, J. T. *J. Am. Chem. Soc.* **1982**, *104*, 55.
(6) Whetten, R. L.; Fu, K. J.; Grant, E. R. *J. Chem. Phys.* **1982**, *77*, 3769.
(7) Miller, M. E.; Grant, E. R. *J. Am. Chem. Soc.* **1984**, *106*, 4635.
(8) Graham, M. A. Ph.D. Thesis, University of Cambridge, 1971.
(9) Hanlan, L.; Huber, H.; Ozin, G. A. *Inorg. Chem.* **1976**, *15*, 2592.
(10) Morton, J. R.; Preston, K. F. *Organometallics* **1984**, *3*, 1386.
(11) Van Zee, R. J.; Bach, S. B. H.; Weltner, W., Jr. *J. Phys. Chem.* **1986**, *90*, 583.
(12) Seder, T. A.; Ouderkirk, A. J.; Weitz, E. *J. Chem. Phys.* **1986**, *85*, 1977.
(13) Seder, T. A.; Church, S. P.; Weitz, E. *J. Am. Chem. Soc.* **1986**, *108*, 4721.
(14) Seder, T. A.; Church, S. P.; Weitz, E. *J. Am. Chem. Soc.* **1986**, *108*, 7518.
(15) Fletcher, T. R.; Rosenfeld, R. N. *J. Am. Chem. Soc.* **1985**, *107*, 2203.
(16) Rayner, D. M.; Nazran, A. S.; Drouin, M.; Hackett, P. A. *J. Phys. Chem.* **1986**, *90*, 2882.
(17) Church, S. P.; Hermann, H.; Grevels, F.-W.; Shaffner, K. *J. Chem. Soc., Chem. Commun.* **1984**, 785.
(18) Church, S. P.; Hermann, H.; Grevels, F.-W.; Shaffner, K. *Inorg. Chem.* **1984**, *23*, 3830.
(19) Klotzbücher, W. E.; Shaffner, K. *J. Chem. Soc., Chem. Commun.* **1985**, 594.
(20) Moore, B. D.; Simpson, M. B.; Poliakoff, M.; Turner, J. J. *J. Chem. Soc., Chem. Commun.* **1984**, 972.

vestigated Cr(CO)₆,[15] and we have reported on the production of the monocarbonyl, CoCO following the photodissociation of Co(CO)₃NO.[16] The general picture that evolves from these studies and from indirect chemical trapping experiments[21] is that, in the gas phase, the ultraviolet photodissociation of M(CO)ₙ may involve the loss of more than one CO ligand, the exact number depending on the excess energy left in the M(CO)ₙ₋₁ fragment after loss of the first ligand. The degree of unsaturation in the photolysis product can therefore be controlled to some extent by the choice of photolysis wavelength. In many cases it is possible to make unambiguous assignments of time-resolved infrared spectra to individual "true" gas-phase species by following their development in time in the presence of added CO. Such an independent assignment of the infrared spectra of gas phase, coordinatively unsaturated carbonyl species is invaluable both in assessing matrix assignments and their extrapolation to gas-phase values and as a test for theories of carbonyl fragment structure.[22-24] These theories refer per se to isolated species although their development was initially stimulated by matrix results.

In view of the disagreement over V(CO)ₓ species in rare-gas matrices and to expand our general knowledge of the gas-phase spectroscopy and reactivity of unsaturated carbonyl species and the photochemistry of transition-metal carbonyls, we have carried out this time-resolved infrared absorption study of the wavelength dependence of the excimer laser photolysis of vanadium hexacarbonyl, V(CO)₆.

Experimental Section

Our time-resolved infrared spectrometer has been described before[16] and only essential features and some minor modifications are discussed here. The photolysis source in these experiments was an excimer laser, either a Lumonics 860-1 (ArF, KrF, XeF) or a Lumonics 861-4 (XeCl). The probe source was an NRC built, line tunable (2033–1655 cm⁻¹), liquid nitrogen cooled, CW CO laser which double passes the 120 mm reaction cell, almost collinear with the photolysis beam. Care was taken to ensure full overlap of the probe beam (∼2 mm diameter) with the ultraviolet irradiated portion of the sample volume (∼8 mm diameter). Transient changes in the absorption of the probe laser beam were monitored by an Infrared Associates fast (∼200 ns risetime) MCT detector/pre-amp whose output was processed as before (Tektronix 7A13 differential amplifier, Biomation 8100 digitizer, DEC LSI 11/23 computer). Improvement in the detector enclosure resulted in reduction of the EMI pickup from the photolysis laser to a negligible level. Fifty shots were averaged to record each kinetic trace. Time-resolved infrared difference absorption spectra were constructed from a series of kinetic runs at different probe wavelengths by the computer. Normalization for probe intensity changes between runs was again achieved by chopping the probe beam, synchronously triggering the photolysis laser and using the fast differential amplifier to record small signal changes at high sensitivity simultaneously with total signal strength. CO laser wavelengths were monitored with an Optical Engineering spectrum analyzer. Photolysis pulse energies were measured after the cell with a Scientec power meter and were monitored continuously throughout each run, before and after the cell, with beam splitters and photodiodes.

V(CO)₆ (Morton Thiokol Inc.) was stored at −4 °C, handled only under vacuum or in inert atmosphere and used without further purification. The low vapor pressure of this compound, which is of the order of 0.5 Torr at 25 °C, coupled with the need to flow the gas in order to present a fresh sample for each shot and the need to prevent deposition of final reaction products on the cell windows resulted in the sample system shown in Figure 1. Ar and CO flows were controlled by needle valves. Total gas pressures were monitored with an MKS Baratron capacitance manometer. Relative Ar/CO ratios were measured with an Inficon IQ 200 residual gas analyzer. Typically partial pressures of ∼0.1 Torr of Ar at inlet I and ∼7 Torr of Ar(±CO) at inlet II gave a partial pressure of ∼30 mTorr of V(CO)₆. The latter was monitored by the attenuation of the CW CO laser probe beam.[25]

(21) Yardley, J. T.; Gitlin, B.; Nathanson, G.; Rosan, A. M. *J. Chem. Phys.* **1981**, *74*, 370.

(22) Burdett, J. K. *J. Chem. Soc., Faraday Trans. 2* **1974**, *70*, 1599.

(23) Burdett, J. K. *Inorg. Chem.* **1975**, *14*, 375.

(24) Elian, M.; Hoffmann, R. *Inorg. Chem.* **1975**, *14*, 1058.

(25) The absorption coefficient of V(CO)₆ at 1988 cm⁻¹ was determined by FTIR as $(0.35^{+0.35}_{-0.15})$ Torr⁻¹ cm⁻¹. The large uncertainty in this parameter, due to deposition and/or reaction on the walls of the FTIR cell, affects absolute values of quoted rate constants for reaction with V(CO)₆ and sets confidence limits at a factor of two in either direction from the quoted values.
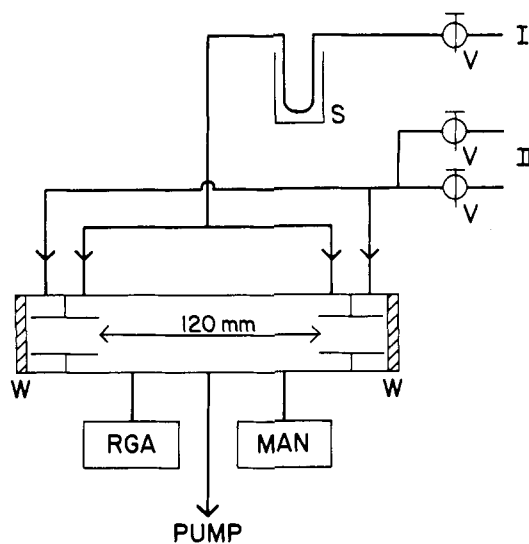
Figure 1. Flow system for low vapor pressure samples: S, sample in U-tube in constant temperature bath; V, needle value; W, calcium fluoride window; RGA, residual gas analyzer; MAN, capacitance manometer.
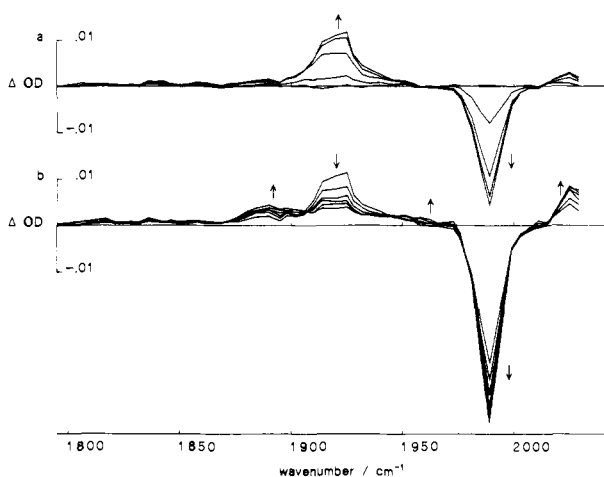

Figure 2. Time-resolved difference absorption spectra following 308-nm photolysis of V(CO)₆ (33 mTorr) in Ar buffer gas (7 Torr): (a) early spectra at 200-ns intervals starting at the photolysis pulse, (b) spectra at 1.5-μs intervals starting 1.5 μs after the photolysis pulse. The arrows indicate the behavior of associated peaks with increasing time.

Results

The excimer laser photolysis of V(CO)₆ was studied at four wavelengths: 193 (ArF), 248 (KrF), 308 (XeCl), and 351 (XeF) nm. The electronic structure of V(CO)₆ is complex with an estimate of over 20 dipole-allowed transitions in the ultraviolet.[26] It is not possible to identify individual levels populated at the above wavelengths. Time-resolved infrared difference absorption spectra were gathered in the absence and presence of added CO, and the kinetic behavior of observed transient peaks was recorded as a function of V(CO)₆, buffer gas, and CO pressure. This raw information finally results in infrared assignments in the CO stretching region for the species V(CO)₃₋₅ and rate constants for the reaction of these species with CO and V(CO)₆.

308-nm Photolysis. There is no bond dissociation energy, E_D, reported for V(CO)₆. However, where known, the transition-metal carbonyls show average E_Ds of 26–43 kcal mol⁻¹[26] and E_D for the loss of a single CO ligand of 37–46 kcal mol⁻¹.[27] Assuming the values for V(CO)₆ to be of the same order and following the pattern set by Fe, Cr, and Co carbonyls we expect 308-nm (93

(26) Holland, G. F.; Manning, M. C.; Ellis, D. E.; Trogler, W. C. *J. Am. Chem. Soc.* **1983**, *105*, 2308.

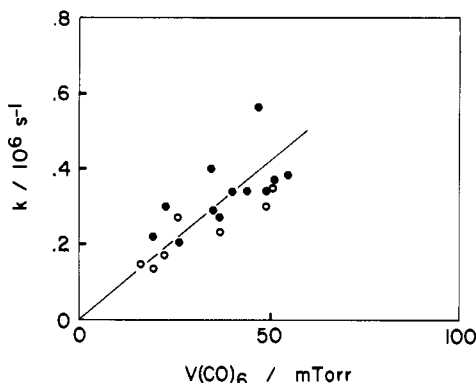(27) Connor, J. A. *Top. Curr. Chem.* **1977**, *71*, 71.

Figure 3. Dependence of the pseudo-first-order rate constant for the primary fragment loss ($\bullet$, 1921 cm^{-1}) and secondary parent loss (O, 1989 cm^{-1}) processes on V(CO)$_6$ pressure in the 308-nm photolysis of V(CO)$_6$.
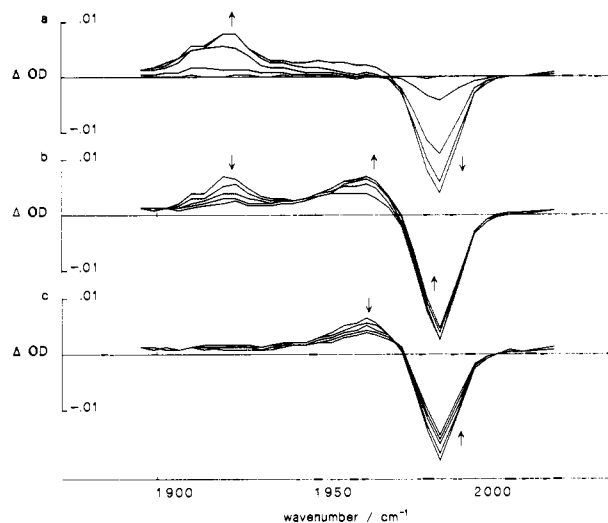

Figure 4. Time-resolved difference absorption spectra following 308-nm photolysis of V(CO)$_6$ (40 mTorr) in the presence of 0.7 Torr of CO and 6.3 Torr of Ar. The interval between consecutive spectra is 0.2 μs: (a) 0–0.8 μs, (b) 1.0–1.8 μs, (c) 2.0–2.8 μs after the photolysis pulse. The arrows indicate the behavior of associated peaks with increasing time.

kcal mol^{-1}) photolysis to result in the probable loss of two CO ligands.

Figure 2 shows time-resolved difference absorption spectra following the 308-nm photolysis of V(CO)$_6$ (35 mTorr) in Ar buffer gas (7 Torr). The main features at early times are an increase in transmission at 1989 cm^{-1}, at a rate matching the upper bandwidth limit of our detection system, and the growth of a single absorption feature at 1920 cm^{-1}. No features were observed in the unreported range below 1800 to 1680 cm^{-1}. V(CO)$_6$ shows a single, relatively broad band in the CO stretching region at 1988 cm^{-1} in its steady-state gas-phase infrared spectrum, which is associated with an O_h geometry undergoing a dynamic Jahn–Teller distortion.[28] The decrease in absorption at 1989 cm^{-1} is plainly due to consumption of parent molecules and the increase at 1920 cm^{-1} to a primary product. Relaxation of nascent internal energy in the primary product fragments from M(CO)$_x$ photolysis by buffer gas is also a general phenomenon in the systems studied to date.[12–16] In the case of V(CO)$_6$ it is not marked, but closer examination of the development of the 1920-cm^{-1} absorption shows a slight shift to the blue with time. Experiments at 14 and 1.4 Torr of Ar buffer gas pressure, which showed the shift occurring on consistently shorter and longer time scales, respectively, confirmed its attribution to collisional relaxation.

At longer times the primary transient in Figure 2 is seen to decay while new, secondary, transient absorptions grow in at 1890, 1965, and 2025 cm^{-1}. The 1965-cm^{-1} absorption is very weak but its appearance is reproducible. On the same time scale further, secondary, loss of parent absorption occurs at 1989 cm^{-1}. Again this behavior is typical of unsaturated carbonyls and is interpreted as reaction of the primary fragment with parent molecules to form a binuclear complex. This is confirmed by the isobestic points observed at 1905, 1949, and 2015 cm^{-1} in the changing transient absorption spectra of Figure 2 and by the kinetic behavior of primary fragment loss and secondary parent loss illustrated in Figure 3. This figure shows the dependence of the first-order rate constants for both processes, found from single exponential fits, on V(CO)$_6$ pressure. Both sets of results show the same linear behavior and from them we obtain the value (2.4 $\pm$ 0.6) $\times$ 10^{-10} cm^3 molecule^{-1} s^{-1} for the bimolecular rate constant for the reaction between the primary fragment, shown below to be V(CO)$_4$, and parent. The quoted error is the statistical error from the linear fit. Confidence limits for the absolute value of this rate constant of a factor of 2 in either direction are set by those placed on the absorption coefficient of V(CO)$_6$.[25]
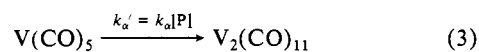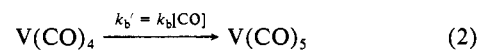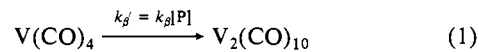
308-nm Photolysis with Added CO. Figure 4 shows time-resolved difference absorption spectra following the 308-nm photolysis of V(CO)$_6$ (40 mTorr) in the presence of 0.7 Torr of CO and 6.3 Torr of Ar. At early times the behavior is similar to that observed without CO: there is an increase in transmission at 1989 cm^{-1} associated with parent depletion and a primary fragment absorbing at 1920 cm^{-1} is again observed. However, in the

presence of 0.7 Torr of CO the 1920-cm^{-1} absorption peaks at 800 ns and then decays concomitant with the growth of a new transient absorption at 1960 cm^{-1}. In turn the 1960-cm^{-1} absorption peaks at 1.6 μs and then decays, in this case associated with a matching decay in the transient transmission at the parent wavelength. The decay in the transient transmission occurs concertedly over the whole peak as expected from parent recovery rather than production of a further transient absorbing coincidentally close to the parent. These observations are all consistent with the primary fragment sequentially adding two CO molecules to reform parent V(CO)$_6$. This identifies the primary fragment absorbing at 1920 cm^{-1} as V(CO)$_4$ and associates the intermediate 1960-cm^{-1} absorption with V(CO)$_5$. The binuclear complex observed at long times after photolysis in the absence of CO, see above, can then be reasonably assumed to be of the stoichiometry V$_2$(CO)$_{10}$ formed by the combination of V(CO)$_4$ and V(CO)$_6$.

In summary, the 308-nm photolysis of V(CO)$_6$ leads to the loss of two CO ligands and the production of V(CO)$_4$ as the major primary fragment. No other primary fragments are observed. V(CO)$_5$ is formed as an intermediate fragment in the recovery of V(CO)$_6$ in the presence of added CO. This behavior is described by the following kinetic scheme

$$V(CO)_4 \xrightarrow{k_{\beta}' = k_{\beta}[P]} V_2(CO)_{10} \tag{1}$$

$$V(CO)_4 \xrightarrow{k_b' = k_b[CO]} V(CO)_5 \tag{2}$$

$$V(CO)_5 \xrightarrow{k_{\alpha}' = k_{\alpha}[P]} V_2(CO)_{11} \tag{3}$$

$$V(CO)_5 \xrightarrow{k_a' = k_a[CO]} V(CO)_6 \tag{4}$$

where reaction 3 has not been observed directly but has been included for completeness and [P] is the parent concentration. Under pseudo-first-order conditions V(CO)$_4$ is predicted to decay exponentially with a rate constant of (k_{β}[P] + k_b[CO]). k_{β} is already known from the experiments varying [P] in the absence of CO. The decays of the V(CO)$_4$, 1920-cm^{-1} absorption measured in the presence of a series of CO pressures were fitted to a single exponential, and the resulting linear dependance of the observed rate constant on [CO] at fixed [P] leads to a value for k_b, the rate constant for reaction of CO with V(CO)$_4$, of (0.5 $\pm$ 0.1) $\times$ 10^{-10} cm^3 molecule^{-1} s^{-1}. The predicted time dependance of V(CO)$_5$ concentration is given by

$$[V(CO)_5] = \frac{B_0 k_b[CO](e^{-k_A t} - e^{-k_B t})}{k_B - k_A}$$

(28) Lewis, K. E.; Golden, D. M.; Smith, G. P. *J. Am. Chem. Soc.* **1984**, *106*, 3905.

where $k_A = k_\alpha[P] + k_a[CO]$ and $k_B = k_\beta[P] + k_b[CO]$ and B_0 is the initial concentration of $V(CO)_4$. At long time $[V(CO)_5]$ decay approaches single exponential with a rate corresponding to the smaller of k_A and k_B. Under conditions of excess parent molecules the time dependancy of the change in parent concentration, $\Delta[V(CO)_6]$, is governed not only by recovery through reaction 4 but also by further loss through reactions 1 and 3 such that

$$\Delta[V(CO)_6] = B_0 \left\{ \frac{(k_a' - k_\alpha')k_b'}{k_A k_B} - \frac{k_\beta'}{k_B} - \left(\frac{k_a' - k_\alpha'}{k_A - k_B} - k_\beta' \right) \frac{e^{-k_b t}}{k_B} + \frac{(k_a' - k_\alpha')k_b' e^{-k_a t}}{(k_A - k_B)k_A} - 1 \right\}$$

where $\Delta[V(CO)_6]$ is measured from the parent initial concentration before irradiation. The final level to which the parent absorption recovers is given by

$$\Delta[V(CO)_6] = B_0 \left\{ \frac{(k_a' - k_\alpha)k_b'}{k_A k_B} - \frac{k_\beta}{k_B} - 1 \right\}$$

and the signal recovery to this level approaches single exponential at long time with a rate again corresponding to the smaller of k_A and k_B; that is providing [CO] is in sufficient excess for a degree of recovery to take place. Single exponential fits were made to the tails of the $V(CO)_5$, 1960-cm⁻¹ decays and to the tails of the parent absorption recoveries at a series of CO pressures. Both sets of observed rate constants showed, within error, the same linear dependance on [CO] and lead to a value for the smaller of k_a or k_b of $(0.5 \pm 0.1) \times 10^{-10}$ cm³ molecule⁻¹ s⁻¹. This value is the same, within error, as that credited to k_b from measurements on the CO dependance of $V(CO)_4$ decay implying that $k_a \geq k_b$. Final limits on k_a can be found by considering the time, t_{max}, taken for $[V(CO)_5]$ to reach its maximum which is given by

$$t_{max} = \frac{\ln(k_A/k_B)}{k_A - k_B}$$

and at the limit of $k_A = k_B$ becomes

$$t_{max} = 1/k_A$$

At relatively high CO pressures we find $1/t_{max}$ for the $V(CO)_5$, 1965-cm⁻¹ absorption to match, within error, the values found for the rate of decay of $V(CO)_4$ and $V(CO)_5$ and of recovery of $V(CO)_6$ showing that $k_A = k_B$ within error. At the CO pressures used k_A and k_B are dominated by k_a and k_b relatively so that we conclude that $V(CO)_5$ reacts with CO with a rate constant, k_a, of $(0.5 \pm 0.1) \times 10^{-10}$ cm³ molecule⁻¹ s⁻¹.

351-nm Photolysis. At 81 kcal mol⁻¹ the energy of a 351-nm photon is 12 kcal mol⁻¹ less than that of a 308-nm photon. Depending on the specific bond energies it is possible that photolysis at 351 nm will result in the loss of one fewer CO ligands. Such behavior has been reported for $Cr(CO)_6$[13] (although the difference there was between 248- and 308-nm photolysis). This is not the case here as seen in Figure 5, which shows the transient absorption behavior following $V(CO)_6$ (80 mTorr) photolysis at 351 nm in Ar (7 Torr) buffer gas to be almost identical with that at 308 nm, with a primary fragment again formed at 1920 cm⁻¹, which reacts with parent molecules to produce a binuclear complex with absorption peaks at 1890, 1965, and 2025 cm⁻¹. The bimolecular rate constant for this process matched, within error, that found at 308 nm. The only difference between the 351- and 308-nm results is the absence of any observable effect of Ar buffer gas pressure on the development of the 1920-cm⁻¹ primary fragment at the longer wavelength. This is consistent with the lower energy of the 351-nm photon and suggests that the threshold for removal of two CO ligands is not much lower than 81 kcal mol⁻¹. The limits that these results put on E_D values are discussed below.

248-nm Photolysis. Although photolysis at 351 and 308 nm gives essentially the same outcome, the outcome of 248-nm photolysis is markedly different as can be seen in the transient
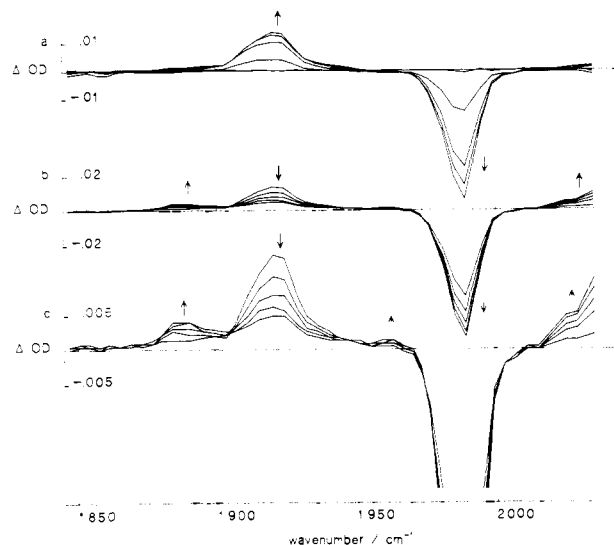

Figure 5. Time-resolved difference absorption spectra following 351-nm photolysis of $V(CO)_6$ (80 mTorr) in Ar buffer gas (7 Torr): (a) early spectra at 200-ns intervals starting coincident with the photolysis pulse, (b) spectra at 1.5-μs intervals starting 1.5 μs after the photolysis pulse, and (c) spectra shown at 1.5-μs intervals as in part b expanded vertically by a factor of 4. The arrows indicate the behavior of associated peaks with increasing time.
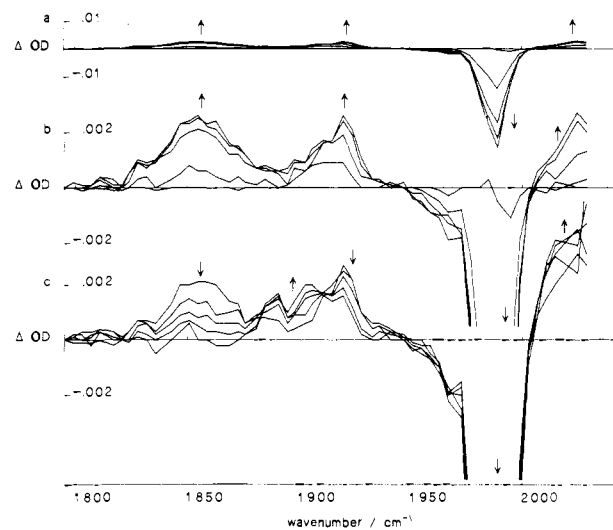

Figure 6. Time-resolved difference absorption spectra following 248-nm photolysis of $V(CO)_6$ (40 mTorr) in Ar buffer gas (7 Torr): (a) early spectra at 200-ns intervals starting coincident with the photolysis pulse, (b) early spectra at 200-ns intervals on an expanded vertical scale (×10), and (c) spectra at 1.5-μs intervals starting 1.5 μs after the photolysis pulse. The arrows indicate the behavior of associated peaks with increasing time.

absorption spectra shown in Figure 6 which result from the 248-nm photolysis of $V(CO)_6$ (40 mTorr) in Ar (7 Torr) buffer gas. The early spectra show parent depletion at 1989 cm⁻¹ as before but now there are three peaks, at 1859, 1920, and 2025 cm⁻¹, which can be attributed to a primary fragment or fragments. The overall transient absorption shown by these peaks is small compared to the transient transmission at the parent wavelength. This suggests either that the primary fragments have relatively low extinction coefficients or that there is another, primary, "dark" fragment which our experiment does not detect. Although the spectra in Figure 6 are shown over the range 2033–1795 cm⁻¹ they were collected down to the lower limit of our CO laser at 1655 cm⁻¹. No features were observed in the nonreported region.

At longer times the primary fragments decay as new absorptions at 1880 and 1905 cm⁻¹ grow and changes in the band originally at 2025 cm⁻¹ are observed. The time scale for these effects is
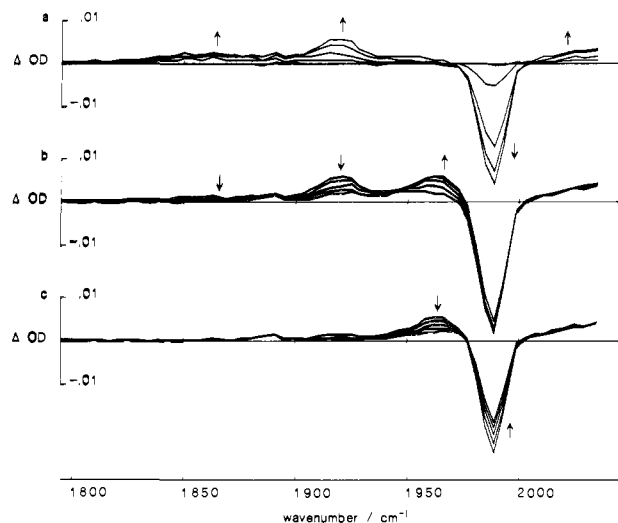
Figure 7. Time-resolved difference absorption spectra following 248-nm photolysis of $V(CO)_6$ (40 mTorr) in the presence of 1 Torr of CO and 6 Torr of Ar. The interval between consecutive spectra is 0.2 μs: (a) 0–0.8 μs, (b) 1.0–1.8 μs, and (c) 2.0–2.8 μs after the photolysis pulse. The arrows indicate the behavior of associated peaks with increasing time.

Figure 8. Time dependence of absorption features identified with $V(CO)_x$ ($x = 3$ to 6) species following the 248-nm photolysis of $V(CO)_6$ in the presence of 1 Torr of CO and 6 Torr of Ar. Curves are labeled by x and were monitored at the wavelengths given in Table I. The dashed line shows the behavior of the peak attributed to $V(CO)_5$ after correction for overlapping parent absorption.

consistent with reaction of the primary fragment(s) with parent molecules. Another major difference with photolysis at longer wavelengths emerges here as the secondary chemistry is demonstrably more complex. Besides the possibility of there being more than one primary fragment it also appears that the binuclear species produced by reaction of primary fragments with $V(CO)_6$ are themselves reactive with parent molecules. This topic of organometallic chain reactions, metal carbonyl polymerization, and metal carbonyl cluster formation will be the subject of a separate paper reporting experiments designed to probe the longer time consequences of $V(CO)_6$ photolysis. Here we note that the decay of the 1859-cm^{-1} primary fragment, shown below to be $V(CO)_3$, was found to be single exponential and to decay with a $V(CO)_6$ pressure-dependant rate constant of $(3.1 \pm 0.7) \times 10^{-10}$ cm^3 molecule^{-1} s^{-1}[25] and that the secondary increase in absorption at 1905 and 2015 cm^{-1} matches this rate within error.

248-nm Photolysis with Added CO. Figure 7 shows time-resolved difference absorption spectra following the 248-nm photolysis of $V(CO)_6$ (40 mTorr) in the presence of 1 Torr of CO and 6 Torr of Ar. As in the absence of CO, initial transient absorptions at 1859, 1920, and 2025 cm^{-1} accompany the fast loss of absorption at the parent wavelength. The last of these is at the limit of our spectral range and may peak further to the blue. However, in the presence of 1 Torr of CO, the broad absorption centered at 1859 cm^{-1} reaches its maximum after 500 ns and then decays accompanied by the growth of a relatively strong absorption at 1920 cm^{-1} which matches that assigned to $V(CO)_4$ on the strength of the 308- and 351-nm photolysis results. In turn the 1920-cm^{-1} transient peaks after 900 ns and then decays accompanied by the growth of an absorption of comparable strength at 1960 cm^{-1}. Finally the 1960-cm^{-1} transient peaks after 1.8 μs and then decays, accompanied by recovery of absorption at the parent wavelength, fully consistent with its assignment to $V(CO)_5$ as in the case of 308- and 351-nm photolysis. This is further demonstrated by the time dependence of the relevant transient absorptions shown in Figure 8. This behavior then firmly links the relatively broad absorption at 1859 cm^{-1} with $V(CO)_3$. Of the other initial absorptions, the 2025-cm^{-1} peak shows contour and early growth characteristics, peaking after 600 ns, which are essentially independent of added CO. In the absence of CO the fate of this transient is obscurred by overlap with the product(s) of nucleation reactions, but in the presence of sufficient CO to suppress these reactions the 2025-cm^{-1} absorption, once established, remains unchanged for 6 μs after which it shows sign of slowly splitting into two bands. The 2025-cm^{-1} absorption is not therefore an additional band of $V(CO)_3$ but must be assigned to
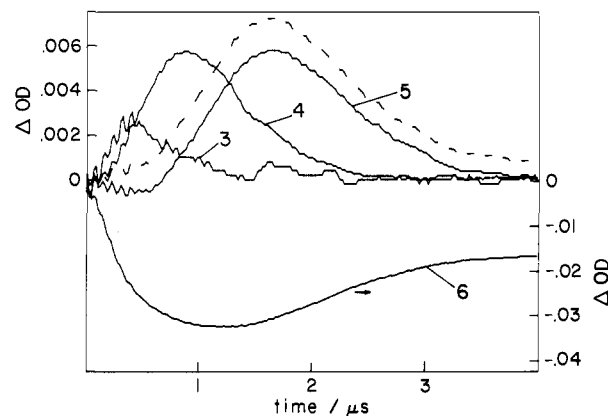
a separate primary product which is relatively unreactive with CO. However, we cannot assign it to any $V(CO)_x$ species with certainty as there remains the possibility that it is "hot" $CO(v = 3)$ which cannot be ruled out on spectroscopic or kinetic grounds. The reported rate of 0.03×10^{-10} cm^3 molecule^{-1} s^{-1} for V–V energy transfer between $CO(v = 3)$ and $CO(v = 0)$[29] would be consistent with the time behavior of the 2025-cm^{-1} transient. Transient absorption at 2066 cm^{-1} has been attributed to $CO(v = 2)$ in the 248-nm photolysis of $Fe(CO)_5$.[12] If the 2025-cm^{-1} absorption is associated with a $V(CO)_x$ species then the most plausible candidate is $V(CO)_2$. The initial absorption at 1920 cm^{-1} is at the wavenumber assigned above to $V(CO)_4$. However, from the addition of CO we conclude $V(CO)_4$ can only be formed with relatively low yield otherwise absorption due to $V(CO)_5$ should appear earlier than seen in Figure 8 despite the fact that at 1960 cm^{-1}, where $V(CO)_5$ was monitored, there is a small obscurring contribution from parent consumption. The 1920-cm^{-1} absorption must then be associated with $V(CO)_3$, with which its kinetic behavior is consistent, or another primary fragment. We disfavor the latter, which could only be $V(CO)_2$ or $V(CO)$, because of the expectation that their reaction with CO will be spin forbidden and therefore relatively slow in contradiction to the observed fast recovery of the 1920-cm^{-1} absorption to the base line in the presence of CO. The single exponential decay of the 1859-cm^{-1} $V(CO)_3$ absorption is also evidence that the 1920-cm^{-1} carrier cannot react with CO to form $V(CO)_3$ on the time scale of its decay.

In summary, 248-nm photolysis of $V(CO)_6$ results in the production of $V(CO)_3$ as a primary fragment, absorbing at 1859 and 1920 cm^{-1}. The absorption at ~ 2030 cm^{-1} is due either to $V(CO)_2$ with a slow rate for the addition of CO or to $CO(v = 3)$. The following reactions describe the fate of these species in the presence of CO.

$$V(CO)_2 \xrightarrow{k_b[P]} V_2(CO)_8 \qquad (5)$$

$$V(CO)_2 \xrightarrow{k_a[CO]} V(CO)_3 \qquad (6)$$

$$V(CO)_3 \xrightarrow{k_\gamma[P]} V_2(CO)_9 \qquad (7)$$

$$V(CO)_3 \xrightarrow{k_c[CO]} V(CO)_4 \qquad (8)$$

With reactions 1–4 they form a complete description of the system. The measurement of $k_\gamma = (3.1 \pm 0.6) \times 10^{-10}$ cm^3 molecule^{-1} s^{-1} has already been discussed in the absence of added CO. Note that if $V(CO)_2$ is formed the limited evidence requires $k_d \ll k_c$, k_b, k_a. Analytical solutions for the time dependence of $V(CO)_x$

---

(29) Haas, H.; Sheline, R. K. *J. Am. Chem. Soc.* **1966**, *88*, 3219.
(30) Deleon, R. L.; Rich, J. W. *Chem. Phys.* **1986**, *107*, 283.

Excimer Laser Photolysis of V(CO)₆

J. Am. Chem. Soc., Vol. 109, No. 22, 1987 6649

Table I. Infrared Absorption Frequencies (cm^{-1}) of Vanadium Carbonyls

	this work, gas phase	ref 28	ref 9, low-temp matrix
$V(CO)_6$		1988	
$V(CO)_5$	1965		1952/1943
$V(CO)_4$	1920		1893
$V(CO)_3$	1859/(1920)[a]		1920
$V(CO)_2$	(2025)[a]		1974–1719[b]
$V_2(CO)_{10}$	1890, 1965, 2025		

[a] This assignment is tentative, see text. [b] Five frequencies were associated with $V(CO)_2$ stoichiometry and assigned to three geometric isomers.

Table II. Bimolecular Rate Constants (10^{-10} cm^3 molecule^{-1} s^{-1}) for the Reaction of Vanadium Carbonyls with $V(CO)_6$ and CO

	$V(CO)_6$[a]	CO
$V(CO)_5$		0.5 ± 0.1
$V(CO)_4$	2.4 ± 0.6	0.5 ± 0.1
$V(CO)_3$	3.1 ± 0.7	0.4 ± 0.1
$V(CO)_2$	<0.5[b]	<0.05[b]

[a] The quoted error is one standard deviation from the linear fit. Confidence limits in absolute values depend on the reliability of the absorption coefficient of $V(CO)_6$.[25] [b] Estimated upper limits for the reaction of the carrier of the 2025-cm^{-1} absorption. There is a possibility that this is CO($v = 3$) not $V(CO)_2$.

concentrations exist, but the expressions are complex and not easily related to experimental data directly. Only salient features are given here. The above condition on k_d, or the lack of production of $V(CO)_2$, allows simplifications which predict $V(CO)_3$ to decay exponentially with a rate constant of $(k_\gamma[P] + k_c[CO])$. The decays of the $V(CO)_3$, 1860-cm^{-1} absorption measured in the presence of a series of CO pressures were fitted to a single exponential, and the resulting linear dependence of the observed rate constant on [CO] leads to a value for k_c of $(0.4 \pm 0.1) \times 10^{-10}$ cm^3 molecule^{-1} s^{-1} which is only slightly less than the value of $(0.5 \pm 0.1) \times 10^{-10}$ cm^3 molecule^{-1} s^{-1} found for k_a and k_b. As with the two-step recovery mechanism detailed explicitly for 308-nm photolysis the parent absorption is predicted to recover in the long time limit at a first-order rate with the rate constant of the slowest step. The parent absorption recovery curves were measured at 1994 cm^{-1} at a series of CO pressures and their tails were fitted to single exponentials. The resulting linear dependence of the observed rate constant on [CO] leads to a bimolecular recovery rate of $(0.4 \pm 0.1) \times 10^{-10}$ cm^3 molecule^{-1} s^{-1} which matches k_c within error.

The behavior of the absorption at 2025 cm^{-1} assigned to $V(CO)_2$ or CO($v = 3$) puts limits of $<0.05 \times 10^{-10}$ cm^3 molecule^{-1} s^{-1} on the reaction of its carrier with $V(CO)_6$ and $<0.5 \times 10^{-10}$ cm^3 molecule^{-1} s^{-1} on the reaction with CO.

193-nm Photolysis. At 193 nm only parent depletion was observed. No transient absorptions were seen over the entire wavelength range. The addition of 1.0 Torr of CO produced no observable absorptions either, although some recovery of parent absorption was seen. Our inability to observe transient fragments at 193 nm may be due to low levels of production caused by the low extinction coefficient of $V(CO)_6$ at that wavelength coupled

with the low infrared absorption cross sections apparently associated with the smaller members of the $V(CO)_x$ series as seen in 248-nm photolysis. Vanadium atoms are also transparent to our experiment.

Fluence Dependence. The effect of photolysis laser fluence on the initial yield of primary fragments and on the depletion of parent was investigated at all wavelengths but 193 nm. In the cases of 351 and 308 nm yields of $V(CO)_4$ and parent depletion were found to depend linearly on fluence from 0 to 4 mJ cm^{-2}. At 248 nm only parent depletion was studied, this time over the range 0–1.5 mJ cm^{-2}, and it was also linear with fluence. The results imply that a single-photon mechanism is in operation at 248, 308, and 351 nm at moderate fluences. In all other studies reported here a fluence of about 1 mJ cm^{-2} was used.

Summary of Results. The final infrared assignments for the $V(CO)_x$ species resulting from this work are given in the first row of Table I. They are based on kinetic arguments that are supported by quantitative measurements of bimolecular rate constants for reactions of $V(CO)_x$ species with CO and $V(CO)_6$. These are listed in Table II.

Discussion

Infrared Assignments. As pointed out in the introduction there is already disagreement between $V(CO)_x$ structures derived from low-temperature co-condensation infrared absorption studies and those derived from ESR measurements. Our assignments for gas-phase $V(CO)_x$ are also in major disagreement with the earlier infrared assignments as seen in Table I. The kinetic arguments behind our assignments are compelling and lead to the conclusion that $V(CO)_x$ structures in the co-condensation experiment are distorted significantly by interaction with the matrix or have been assigned to the wrong stoichiometry. That three different structural isomers of $V(CO)_2$ were invoked to account for all peaks assigned to that stoichiometry may also be indicative of large matrix effects, the availability of different sites, and interference from $V_x(CO)_y$ species.

This doubt thrown on the low temperature matrix infrared assignments is disappointing as most of the information used to test theoretical treatments of the structure of metal carbonyl fragments has come from that source. Also we, and others, have relied in the past on matrix assignments to assist in the assignment of gas-phase transient infrared spectra. We are currently reexamining earlier work on other systems stressing kinetic measurements with CO as an assignment aid in order to determine if the discrepancies are unique to the vanadium system or more widespread.

$V(CO)_x$ Structure. Table III details the geometries of vanadium carbonyl species obtained in previous experimental and theoretical studies. Discrepancies are apparent. Our CO addition experiment supplies unambiguous stoichiometries for species associated with observed transitions. In addition, conclusions concerning the spin state of the transient species can be drawn from the kinetic measurements. Weitz and co-workers have argued convincingly that the rate of CO addition to $M(CO)_x$ species is controlled in the high-pressure limit by spin conservation considerations.[12] Their conclusions are based on the observation of a ca. 500 times slower rate of addition of CO to $Fe(CO)_4$, which involves a triplet to singlet spin flip, compared to that of addition to $Fe(CO)_2$ and

Table III. Comparison of Structural Information on Vanadium Carbonyls from Theory and Experiment

		$V(CO)_5$	$V(CO)_4$	$V(CO)_3$	$V(CO)_2$
this work	gas-phase infrared	low spin	low spin	low spin	(higher spin)
Hanlan, Huber, and Ozin[9]	low-temp rare gas matrix IR	D_{3h}	T_d or D_{4h}	D_{3h}	3 geometric isomers, 2 bent V–C–O
Morton and Preston[10]	low-temp rare gas matrix ESR	C_{2v} low spin	T_d high spin		
Van Zee, Bach, and Weltner[11]	low-temp rare gas matrix ESR			D_{3h} or low spin	C_{2v} int. spin
Burdett[22]	theor, minimum internal energy	D_{3h} low spin	C_{2v} low spin	C_{3v} low spin	C_{2v} low and int. spin
		D_{4h} int. spin	C_{2v} int. spin		
		T_d high spin	D_{3h} high spin		
Burdett[23]	theor hole-pair overlap	C_{4v} low spin	C_{2v} low spin	C_{3v} low spin	C_{2v} low spin
	theor Jahn–Teller considerations[9,22,24]	C_{2v} low spin	C_{2v} low spin	C_{3v} low spin	C_{2v} low spin
Elian and Hoffman[24]	theor MO	C_{4v}	C_{2v}	C_{3v} low spin	

Fe(CO)$_3$ where spin is conserved. The latter proceed at near gas kinetic rates as do the spin-allowed additions of CO to Cr(CO)$_{4-5}$[11] and Co(CO)$_{1-3}$.[16] We find (Table II) that CO reacts with the species V(CO)$_{3-5}$ at a rate comparable to that of the above spin conserving reactions. This is strong evidence that V(CO)$_{3-6}$ all have ground states of the same multiplicity. V(CO)$_6$ has been studied by many groups and by many techniques and undoubtedly has a low spin, doublet ground state although the complete electronic structure is still subject to debate.[26] We therefore conclude that V(CO)$_{3-5}$ also all have low spin, doublet ground states. This is in agreement with the molecular orbital calculations (Table III).

There is some agreement on the structure of V(CO)$_5$ in low-temperature matrices between the two infrared and the ESR measurements. From ESR spectra taken following γ-ray and ultraviolet irradiation of V(CO)$_6$ in Kr Morton and Preston predict a C_{2v} symmetry, slightly distorted from the D_{3h}, trigonal-bipyramidal form, for V(CO)$_5$.[10] The infrared assignments, if they are stoichiometrically correct, imply a D_{3h} structure but would feasibly be insensitive to the slight distortion. However, we are also forced to question the unambiguity of the V(CO)$_5$ ESR assignment below, and this apparent agreement must be viewed as just that. In the gas phase we observe a single infrared band for V(CO)$_5$ shifted 12 cm^{-1} to the blue of the mean of the two V(CO)$_5$ peaks in an Ar matrix. This shift is over two times that predicted by linear extrapolation of Ozin and co-workers's results[9] in Ar, Kr, and Xe to zero polarizability and is therefore rather large to attribute the matrix results to nonspecific matrix interactions. If the infrared and ESR assignments are stoichiometrically correct we are left with the conclusion that matrix effects must stabilize the nearly trigonal-bipyramidal form of V(CO)$_5$ through specific interaction. Molecular orbital calculations are in disagreement, between low spin D_{3h} and C_{4v}, over the lowest energy configuration of V(CO)$_5$ (Table III), indicating that both are low lying and matrix stabilization of either form is energetically conceivable. The broad absorption shown by V(CO)$_5$ in the gas phase is then either the observable feature due to a C_{2v} configuration or it is explained by a dynamic Jahn–Teller distortion of the lower of the two more symmetrical D_{3h} and C_{4v} configurations.

In the same ESR study Morton and Preston assigned a high-spin ($^6A_1$) T_d, tetrahedral structure to V(CO)$_4$. The matrix infrared spectra, even if correcltly assigned, of V(CO)$_4$ was inconclusive as to structure. Our finding of a low-spin ground state for gas-phase V(CO)$_4$ is in direct disagreement with the high-spin ESR assignment. Either the ESR assignment is wrong or surprisingly large specific matrix effects stabilize the T_d form of V(CO)$_4$ in Kr matrices. The ESR spectrum assigned to V(CO)$_5$ only showed evidence that the carrier contained at least two pairs of equivalent carbon atoms from its ^{13}C hyperfine structure. V(CO)$_4$ structure was ruled out on the expectation of a high spin state with four equivalent carbon atoms, through analogy with Cr(CO)$_4^+$. In the light of theoretical predictions of a low spin, C_{2v} structure, and our kinetic evidence for low-spin V(CO)$_4$ it is equally possible that the carrier assigned to V(CO)$_5$ in the ESR experiments was actually C_{2v} V(CO)$_4$.

From ESR spectra of species formed by the reaction of vanadium atoms with CO in rare gas matrices at 4 K Weltner and co-workers found V(CO)$_3$ to be definitely of low spin and to be probably of D_{3h} planar symmetry or possibly C_{3v} pyramidal.[11] The molecular orbital theories predict a C_{3v} structure for low-spin V(CO)$_3$. Our kinetic results confirm V(CO)$_3$ as having a doublet ground state. In the same study they found V(CO)$_2$ to have a quartet ground state.

V(CO)$_6$ Photodissociation Dynamics. V(CO)$_6$ gas phase, ultraviolet photodissociation at moderate fluences follows closely the pattern for metal carbonyls established recently by similar time-resolved infrared absorption studies on Fe(CO)$_5$,[12] Cr(CO)$_5$,[13,15] and Co(CO)$_3$NO.[16] Photon energy is the major factor

in determining the outcome of V(CO)$_6$ photolysis, i.e., the higher the energy of the photon the more ligands are lost. This is consistent with a sequential mechanism involving spontaneous unimolecular dissociation of hot primary fragments. The production of V(CO)$_{3,4,5}$, which all prove to be low-spin doublets in their ground state, can proceed directly through a set of doublet manifolds. The electronic absorption spectrum of V(CO)$_6$ is complex with an estimate of over 20 dipole-allowed transitions in the ultraviolet absorption spectrum.[26] It is therefore not possible to identify individual V(CO)$_6$ excited states populated at excimer laser wavelengths and predict a likely pathway as is possible for Fe(CO)$_5$ where some evidence for wavelength dependence of photolysis outcome due to selective population of initial excited states has been presented.[12]

Bond-Dissociation Energies. From the wavelength dependence of the product fragment distribution we can put limits on the bond-dissociation energies E_{Dx} for CO loss from V(CO)$_x$ species. The observation of V(CO)$_4$ production by 351-nm photolysis puts $(E_{D6} + E_{D5}) < 81$ kcal mol^{-1}. Lack of evidence from buffer gas relaxation studies for appreciable internal energy partitioned to the nascent V(CO)$_4$ following 351-nm photolysis in contrast to its observation at 308 nm suggests that $(E_{D6} + E_{D5})$ is in fact close to 81 kcal mol^{-1}. Failure to remove a further CO ligand at 308 nm puts $(E_{D6} + E_{D5} + E_{D4}) > 93$ kcal mol^{-1}. The observation of V(CO)$_3$ production by 248-nm photolysis puts $(E_{D6} + E_{D5} + E_{D4}) < 148$ kcal mol^{-1} leading to $(E_{D4}) < 67$ kcal mol^{-1}. As a simplification we can conclude that the average bond-dissociation energy for V(CO)$_6$ is in the range 30–40 kcal mol^{-1}, which is consistent with the values of 26–43 kcal mol^{-1} measured for other metal carbonyls.[26]

Conclusions

The gas-phase ultraviolet photolysis of V(CO)$_6$ follows the pattern recently established for the photolysis of metal carbonyls through studies on Fe(CO)$_5$, Cr(CO)$_6$, and Co(CO)$_3$NO. Independent infrared assignments for the species V(CO)$_{3-5}$ based on kinetic measurements of the evolution of the system in the presence of added CO are in major disagreement with low-temperature matrix infrared and ESR studies. The use of the latter to support theories of metal carbonyl fragment structure must be taken with caution.

This study also highlights some of the advantages and limitations of CO laser based time-resolved infrared spectroscopy. Our instrument is capable of detecting transient absorbances of <0.5 × 10^{-3}, a figure that matches many steady-state instruments. However, due to experimental restraints on fragment yields this resolution often only results in a signal-to-noise ratio of 20 for the most prominent transient absorption features. In conjunction with the restricted wavelength range (in our case 1655–2035 cm^{-1}) and discrete wavelength coverage (steps of ~4 cm^{-1}) of such instruments this makes the transient absorption spectra of limited use in assigning geometries to unsaturated carbonyl fragments. The necessary detail available from steady-state spectroscopy of low-temperature matrices and liquid rare gas solutions, including extensive isotope studies, cannot be matched in CO laser based studies of gas-phase fragments.

An advantage of CO laser TRIS is that unambiguous assignments of transient stoichiometry can be made for gas-phase species, as demonstrated here, by following the successive addition of CO. This information complements that available from low-temperature studies in that it indicates if structures established in matrices are retained by the "naked" gas-phase species, as found for Cr(CO)$_5$, or not, as found in this work on V(CO)$_x$. Perhaps more importantly it also allows optimization of photolysis conditions for the production of particular unsaturated organometallic species and provides a method for monitoring their reactivity through both their own disappearance and the appearance of CO-containing products.